

Testing growth rate dependence in cosmological perturbation theory using scale-free models

Azrul Pohan,^{1,2,*} Michael Joyce,¹ David Benhaiem,¹ and Francesco Sylos Labini³

¹*Laboratoire de Physique Nucléaire et de Hautes Energies, UPMC IN2P3 CNRS UMR 7585, Sorbonne Université, 4, place Jussieu, 75252 Paris Cedex 05, France*

²*Laboratory of Theoretical Physics, Institut Teknologi Sumatera, Lampung 35365, Indonesia*

³*Centro Ricerche Enrico Fermi, Via Panisperna 89a, I-00184, Roma, Italy*

We generalize previously derived analytic results for the one-loop power spectrum (PS) in scale-free models (with linear PS $P(k) \propto k^n$) to a broader class of such models in which part of the matter-like component driving the Einstein de Sitter expansion does not cluster. These models can be conveniently parametrized by α , the constant logarithmic linear growth rate of fluctuations (with $\alpha = 1$ in the usual case). For $-3 < n < -1$, where the one-loop PS is both infrared and ultraviolet convergent and thus explicitly self-similar, it is characterized conveniently by a single numerical coefficient $c(n, \alpha)$. We compare the analytical predictions for $c(n = -2, \alpha)$ with results from a suite of N -body simulations with $\alpha \in [0.25, 1]$ performed with an appropriately modified version of the Gadget code. Although the simulations are of small (256^3) boxes, the constraint of self-similarity allows the identification of the converged PS at a level of accuracy sufficient to test the analytical predictions for the α dependence of the evolved PS. Good agreement for the predicted dependence on α of the PS is found. To treat the UV sensitivity of results which grows as one approaches $n = -1$, we derive exact results incorporating a regularisation k_c and obtain expressions for $c(n, \alpha, k_c/k)$. Assuming that this regularisation is compatible with self-similarity allows us to infer a predicted functional form of the PS equivalent to that derived in effective field theory (EFT). The coefficient of the leading EFT correction at one loop has a strong dependence on α , with a change in sign at $\alpha \approx 0.16$, providing a potentially stringent test of EFT.

I. INTRODUCTION

Cosmological perturbation theory (PT) is a very important tool in the theory of cosmological structure formation (for a review, see e.g. [1]). It is essentially the only useful analytical instrument currently available to provide insight into non-linear dynamics, and also an exact benchmark for numerical simulations. Despite its apparent simplicity, it has remained an active area of research over several decades, and there are still open unresolved issues relevant to its application to standard cosmological models. In particular much research has been focused on the sensitivity of the functions describing non-linear corrections at a given (weakly non-linear) scale to contributions from smaller scales. These “ultraviolet” contributions are associated with apparently unphysical divergences in the simplest formulation of PT, and a number of different approaches have been proposed to regulate them (see e.g. [2–23]).

Scale-free models, on the other hand, are a family of simplified cosmological models with initial fluctuations characterized by a power spectrum (PS) and an Einstein de Sitter (EdS) expansion law $a(t) \propto t^{2/3}$. Scale-free models are of interest in the context of perturbation theory — and more generally — because they provide a very well-controlled framework within which to understand and test it against numerical results. This is the case because of the so-called *self-similar evolution* characterising these models, which makes the temporal evolution

of clustering statistics essentially trivial as it is given by a rescaling of the spatial coordinates. This property means that any theoretical predictions which can be made for them will take a much simpler form than in a realistic (e.g. Lambda cold dark matter (LCDM)) cosmology. In perturbation theory, for example, the correction to the PS at each order in perturbation is given by a single number, rather than by a function of scale as in standard models. Further, as has been demonstrated recently [24, 25], this same property of self-similarity allows one to obtain very precise results for statistics from numerical simulations. These models can thus provide a potential test-bed for PT and in particular for the question of their ultraviolet divergences and their regulation.

Scale-free models are usually understood to correspond to a standard EdS cosmology, with source for the expansion being the matter which clusters start from initial Gaussian fluctuations with a PS $P(k) \propto k^n$. This means that one can explore the properties of clustering — and the adequacy of perturbation theory in describing them — as a function of the initial conditions (i.e. of n), but only within the setting of the single EdS cosmology. In this article we consider perturbation theory in a broader class of scale-free models first considered in [26] and which we call here *generalized scale-free models*. In these models the initial fluctuations are still defined by a power-law PS $P(k) \propto k^n$ but the EdS expansion is driven by the energy density of the clustering matter and, additionally, of a smooth matter-like component (with energy density scaling as $1/a^3$). The EdS model is thus one of a one-parameter family of such models. This parameter can be given by the ratio of the energy density of the

* azrul.pohan@lpnhe.in2p3.fr

matter clustering matter to the total energy density, or equivalently, by the linear growth rate of density fluctuations. This allows us to potentially exploit the nice properties of scale-free models to test perturbation theory in a broader setting which probes also dependence on the expansion history, and specifically on the linear growth rate of fluctuations. We focus here on the simplest canonical analysis in perturbation theory, of the one-loop PS. Building on our derivation in [27] (hereafter P1) of the kernels in Eulerian and Lagrangian perturbation theory for the generalized EdS cosmologies, we generalize existing analytical results in standard perturbation theory for the one loop PS in the usual scale-free models to these generalized scale-free models. We analyse the interesting and non-trivial predicted dependences on the growth rate and report some tests of these results against analysis of data from N -body simulations performed with an appropriately modified code developed in [26]. We also discuss how the effective field theory (EFT) approach to the regularisation of ultraviolet divergences is modified in this class of scale-free models and the interesting possible numerical tests these results suggest.

II. POWER SPECTRUM IN GENERALIZED SCALE-FREE MODELS

We consider (as in [26]) models of pressureless matter clustering under its self-gravity starting from density fluctuations which are Gaussian and characterized by a power-law PS $P(k) \propto k^n$. The expanding cosmological background in which it evolves is given by

$$H^2 = \kappa^2 \frac{8\pi G}{3} \rho_m \quad (1)$$

where ρ_m is the density of clustering matter, H is the Hubble expansion rate, and κ^2 is a positive constant. While the physical interpretation of this expansion law is not in practice of any relevance to our considerations here, we note that, as discussed in P1 (see also [26]), for $\kappa^2 > 1$ one can interpret it as arising from the contribution of an additional matter component that does not cluster, while for any κ^2 it can be interpreted in terms of a change in the effective Newton constant governing expansion relative to that governing clustering. Doing the standard analysis of linear perturbation theory using this expansion law we obtain a growth law $D(a) \propto a^\alpha$ where the constant growth rate α is related to κ^2 by the

relation

$$\alpha = -\frac{1}{4} + \frac{1}{4} \sqrt{1 + \frac{24}{\kappa^2}}. \quad (2)$$

Just as in the usual EdS model (with $\kappa^2 = 1$ and $\alpha = 1$), we have an expansion law $a(t) \propto t^{2/3}$ and there is only one characteristic length scale associated with the power-law PS. The property of self-similarity of evolution of clustering follows if such evolution is indeed well-defined without cut-offs in the infrared and ultraviolet. Theoretical analysis (see e.g. [28]) suggest that this can be expected to be true for $-3 < n < 4$, and many different studies using numerical simulations indicate that such self-similarity is indeed observed in at least up to $n = 2$ (see e.g. [26, 29–35]), and irrespective of whether cosmological EdS expansion is supposed or not [36–38]. Indeed a hypothesis underlying numerical simulation in cosmology is that clustering is insensitive to the infrared or ultraviolet cut-offs necessarily introduced by such method (box size, particle density, force smoothing, etc.).

A. Power spectrum in generalized EdS cosmology

We define canonically (and as in P1) the PS $P(\vec{k}) \equiv P(k)$ ($k = |\mathbf{k}|$) of the (assumed) statistically homogeneous and isotropic stochastic density field by

$$\langle \delta(\mathbf{k}, a) \delta(\mathbf{k}', a) \rangle = (2\pi)^3 \delta^{(D)}(\mathbf{k} + \mathbf{k}') P(k, a), \quad (3)$$

where $\langle \dots \rangle$ denotes the ensemble average. We have shown in P1 that, just as for the usual EdS model, the equations describing the clustering of matter in the fluid limit, with irrotational velocity, can be solved, in generalized EdS models (gEdS), with a separable ansatz for the density field:

$$\delta(\mathbf{k}, a) = \sum_{i=1}^{\infty} D^i(a) \delta^{(i)}(\mathbf{k}), \quad (4)$$

and likewise for the velocity perturbations. Assuming that the fluctuations are Gaussian at linear order, one obtains the PS at one loop as

$$P_{1\text{-loop}}(k, a) = P_L(k, a) + 2P_{13}(k, a) + P_{22}(k, a), \quad (5)$$

where $P_L(k, a)$ is the linear power spectrum and the one-loop contributions are

$$P_{13}(k, a) = 3P_L(k, a) \int \frac{d^3q}{(2\pi)^3} P_L(q, a) F_3^{(s)}(\mathbf{k}, \mathbf{q}, -\mathbf{q}), \quad (6)$$

$$P_{22}(k, a) = 2 \int \frac{d^3q}{(2\pi)^3} P_L(q, a) P_L(|\mathbf{k} - \mathbf{q}|, a) |F_2^{(s)}(\mathbf{k} - \mathbf{q}, \mathbf{q})|^2, \quad (7)$$

where the superscript “s” indicates that the kernels F_2 and F_3 are symmetrized with respect to their arguments. These expressions are identical to those in the standard EdS model and the only difference in the gEdS models come

through the modification to the kernels, which (see P1 for detail) are now functions of the parameter α :

$$F_2(\mathbf{q}_1, \mathbf{q}_2) = \left(\frac{1+4\alpha}{1+6\alpha}\right)\tilde{\alpha}(\mathbf{q}_1, \mathbf{q}_2) + \left(\frac{2\alpha}{1+6\alpha}\right)\tilde{\beta}(\mathbf{q}_1, \mathbf{q}_2), \quad (8)$$

$$G_2(\mathbf{q}_1, \mathbf{q}_2) = \left(\frac{1+2\alpha}{1+6\alpha}\right)\tilde{\alpha}(\mathbf{q}_1, \mathbf{q}_2) + \left(\frac{4\alpha}{1+6\alpha}\right)\tilde{\beta}(\mathbf{q}_1, \mathbf{q}_2), \quad (9)$$

$$F_3(\mathbf{q}_1, \mathbf{q}_2, \mathbf{q}_3) = \frac{1}{2} \left\{ \left(\frac{1+6\alpha}{1+8\alpha}\right)\tilde{\alpha}(\mathbf{q}_1, \mathbf{q}_2 + \mathbf{q}_3)F_2(\mathbf{q}_2, \mathbf{q}_3) + \left(\frac{2\alpha}{1+8\alpha}\right)\tilde{\beta}(\mathbf{q}_1, \mathbf{q}_2 + \mathbf{q}_3)G_2(\mathbf{q}_2, \mathbf{q}_3) \right. \\ \left. + \left[\left(\frac{1+6\alpha}{1+8\alpha}\right)\tilde{\alpha}(\mathbf{q}_1 + \mathbf{q}_2, \mathbf{q}_3) + \left(\frac{2\alpha}{1+8\alpha}\right)\tilde{\beta}(\mathbf{q}_1 + \mathbf{q}_2, \mathbf{q}_3) \right] G_2(\mathbf{q}_1, \mathbf{q}_2) \right\}, \quad (10)$$

where

$$\tilde{\alpha}(\mathbf{q}_1, \mathbf{q}_2) = \frac{\mathbf{q}_1 \cdot (\mathbf{q}_1 + \mathbf{q}_2)}{q_1^2}, \quad \tilde{\beta}(\mathbf{q}_1, \mathbf{q}_2) = \frac{1}{2}(\mathbf{q}_1 + \mathbf{q}_2)^2 \frac{\mathbf{q}_1 \cdot \mathbf{q}_2}{q_1^2 q_2^2}. \quad (11)$$

Using these expressions (see P1) the PS at one loop is then expressed in terms of three integrals with α dependent coefficients:

$$P_{22} = M_0 + \frac{1+4\alpha}{1+6\alpha}M_1 + \left(\frac{1+4\alpha}{1+6\alpha}\right)^2 M_2, \\ 2P_{13} = N_0 + \frac{1+2\alpha}{1+8\alpha}N_1 + \frac{2\alpha(1+2\alpha)}{(1+6\alpha)(1+8\alpha)}N_2, \quad (12)$$

where the $M_i(k)$ are the integrals

$$M_i = \frac{1}{8\pi^2}k^3 \int_0^\infty dr \int_{-1}^1 d\mu P_L(kr) \\ \times \frac{P_L(k\sqrt{1+r^2-2\mu r})}{(1+r^2-2\mu r)^2} m_i(r, \mu), \quad (13)$$

with

$$m_0(r, \nu) = (\mu - r)^2, \quad (14)$$

$$m_1(r, \nu) = 4r(\mu - r)(1 - \mu^2), \quad (15)$$

$$m_2(r, \nu) = 4r^2(1 - \mu^2)^2, \quad (16)$$

and the $N_i(k)$ integrals are

$$N_i = \frac{1}{8\pi^2}k^3 P_L(k) \int_0^\infty dr P_L(kr) n_i(r), \quad (17)$$

with

$$n_0 = -\frac{4}{3}, \quad (18)$$

$$n_1 = 1 + \frac{8}{3}r^2 - r^4 + \frac{(r^2 - 1)^3}{2r} \ln \left| \frac{1+r}{1-r} \right|, \quad (19)$$

$$n_2 = \frac{1}{r^2} \left(1 - \frac{8}{3}r^2 - r^4 \right) + \frac{(r^2 - 1)^3}{2r^3} \ln \left| \frac{1+r}{1-r} \right|. \quad (20)$$

The variables r and μ in the integrals have been defined from the momenta in Eqs. (6)-(7) as $r = q/k$ and $\mu = \mathbf{k} \cdot \mathbf{q}/(kq)$.

B. Power spectrum for scale-free initial conditions

We now consider the case that $P_L(k)$ is a simple power law. In order to control carefully for infrared and ultraviolet divergences we introduce cut-offs, taking

$$P_L(k, a) = \begin{cases} AD^2 k^n, & \text{if } \varepsilon \leq k \leq k_c \\ 0, & \text{otherwise} \end{cases} \quad (21)$$

where A is the amplitude of the power spectrum at $a = 1$, $D \equiv a^\alpha$ is the linear growth rate of fluctuations, and ε (k_c) are the infrared (ultraviolet) cut-offs.

We will work with the dimensionless power spectrum, defined canonically as

$$\Delta^2(k) = \frac{k^3 P(k)}{2\pi^2}. \quad (22)$$

The one-loop result in Eq. (5) can then conveniently be rewritten as

$$\Delta_{1-loop}^2(k) = \Delta_L^2 \left[1 + c\left(n, \alpha, \frac{\varepsilon}{k}, \frac{k_c}{k}\right) \Delta_L^2 \right], \quad (23)$$

for $\varepsilon \leq k \leq k_c$, and where $\Delta_L^2(k) = \frac{k^3 P_L(k)}{2\pi^2}$.

The dimensionless constant c in Eq. (23) is then given by

$$c\left(n, \alpha, \frac{\varepsilon}{k}, \frac{k_c}{k}\right) = \hat{M}_0 + \frac{1+4\alpha}{1+6\alpha} \left[\hat{M}_1 + \frac{1+4\alpha}{1+6\alpha} \hat{M}_2 \right] \\ + \hat{N}_0 + \frac{1+2\alpha}{1+8\alpha} \left[\hat{N}_1 + \frac{2\alpha}{1+6\alpha} \hat{N}_2 \right] \quad (24)$$

where the \hat{M}_i and \hat{N}_i are dimensionless integrals:

$$\hat{M}_i = \frac{1}{4} \int_{\varepsilon/k}^{k_c/k} dr r^n \int_{\mu_{min}}^{\mu_{max}} d\mu (1+r^2-2\mu r)^{\frac{n}{2}-2} m_i(r, \mu) \quad (25)$$

$$\hat{N}_i = \frac{1}{4} \int_{\varepsilon/k}^{k_c/k} dr r^n n_i(r) \quad (26)$$

where m_i and n_i are the same functions defined above, and

$$\begin{aligned}\mu_{min}(r) &= \text{Max}\left\{-1, \frac{1+r^2 - (k_c/k)^2}{2r}\right\}, \\ \mu_{max}(r) &= \text{Min}\left\{1, \frac{1+r^2 - (\varepsilon/k)^2}{2r}\right\},\end{aligned}\quad (27)$$

are the angular integration limits.

Defining the characteristic scale k_{NL} by $\Delta_L^2(k_{NL}) \equiv 1$, we have

$$k_{NL}(a) \propto a^{-\frac{2\alpha}{3+\alpha}}, \quad (28)$$

and, given the assumed power-law form,

$$\Delta_L^2 = \left(\frac{k}{k_{NL}}\right)^{(n+3)}. \quad (29)$$

If c remains finite when we take the limits $\varepsilon \rightarrow 0$ and $k_c \rightarrow \infty$, c becomes a function of n and α only, with

$$\Delta_{1-loop}^2(k) = \Delta_L^2 \left[1 + c(n, \alpha) \Delta_L^2\right]. \quad (30)$$

The evolution is then explicitly self-similar in a sense that

$$\Delta^2(k, a) = \Delta^2\left(\frac{k}{k_{NL}(a)}, 1\right) \quad (31)$$

i.e. the temporal evolution of clustering corresponds to a rescaling of the spatial coordinates in proportion to the sole characteristic scale, the non-linearity scale $\propto k_{NL}^{-1}$, defined by the power-law PS.

C. Convergence analysis

By studying the behaviour of the integrals \hat{M}_i and \hat{N}_i in the limit $\varepsilon/k \rightarrow 0$ and $k_c/k \rightarrow \infty$ we can determine their infrared and ultraviolet convergence properties. Following standard analysis, and as discussed also in P1, the two dimensional integrals \hat{M}_i have divergences for certain cases in the limit $\varepsilon/k \rightarrow 0$ at $r = 0$ and $r = 1$. As noted e.g. by [39] the contribution of each is in fact identical because of the symmetry of the integrals (the $r = 1$ divergence corresponds to $|\mathbf{q} - \mathbf{k}| \rightarrow \mathbf{0}$, which is identical to the $r = 0$ contribution after a change in variable). This means that the infra-red behaviour can be determined simply by doubling the $r = 0$ contribution, which can easily be inferred from a Taylor expansion.

Explicitly the leading behaviour as $r \rightarrow 0$ of the integrands of \hat{M}_0 and \hat{N}_0 is $\sim r^n$, leading to divergence for $n \leq -1$, but when summed (and taking into account the factor of two mentioned above) these leading divergences cancel and give a ‘‘safe’’ leading behaviour $\sim r^{n+2}$ i.e. convergence for $n \geq -3$. The integrands of the four integrals $\hat{M}_1, \hat{M}_2, \hat{N}_1, \hat{N}_2$, which contribute to the PS via an α -dependent pre-factor, all have this same safe behaviour. As noted in P1 the overall infra-red convergence for any $n > -3$ thus holds for any α , exactly as in the standard EdS model. This result is expected since

TABLE I. Expansion around $(1/r) = 0$ of the integrands of \hat{M}_i and \hat{N}_i . As in the standard EdS model ($\alpha = 1$) these imply that the one loop PS is divergent for $n > -1$. As discussed in the text, the coefficients of these divergences depend on α and at a specific value ($\alpha \approx 0.16$) the leading divergence vanishes and the one-loop result remains ultraviolet convergent for $n < 1/2$.

expansion of integrand	
\hat{M}_0	$r^{2n-2} \left[\frac{1}{2} + \frac{n^2-3n-2}{12r^2} + O\left(\frac{1}{r}\right)^4 \right]$
\hat{M}_1	$r^{2n-2} \left[-\frac{4}{3} - \frac{2(n^2-3n-4)}{15r^2} + O\left(\frac{1}{r}\right)^4 \right]$
\hat{M}'_2	$r^{2n-2} \left[\frac{16}{15} + \frac{8(n^2-3n-4)}{105r^2} + O\left(\frac{1}{r}\right)^4 \right]$
\hat{N}_0	$-\frac{1}{3}r^n$
\hat{N}_1	$r^n \left[\frac{4}{5} - \frac{4}{35r^2} + O\left(\frac{1}{r}\right)^4 \right]$
\hat{N}'_2	$r^n \left[-\frac{4}{3} + \frac{4}{5r^2} + O\left(\frac{1}{r}\right)^4 \right]$

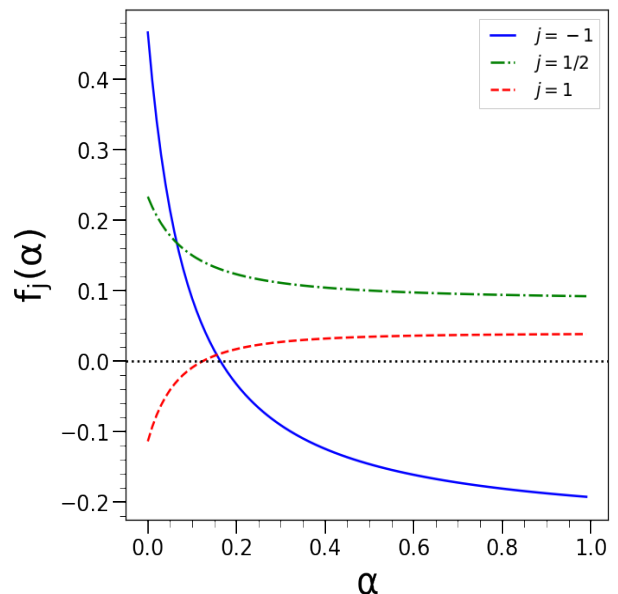


FIG. 1. The pre-factors in Eqs. (32) and (36) for $j = -1, 1/2, 1$ as a function of α . The associated leading UV contribution, which diverges for $n \geq -1$, is proportional to f_{-1} and thus vanishes at $\alpha = \alpha_c \approx 0.16$.

such convergence is a consequence of Galilean invariance [40, 41], a property that is respected by the generalized EdS cosmologies just as in the canonical case.

For $r \rightarrow \infty$, on the other hand, the integrands in $\hat{N}_0, \hat{N}_1, \hat{N}_2$ all have the same leading behaviour $\sim r^n$, and all those in $\hat{M}_0, \hat{M}_1, \hat{M}_2$ the leading behaviour $\sim r^{2n-2}$. For the canonical $\alpha = 1$ case, the one loop PS therefore diverges for $n > -1$ with a leading divergence coming from the term $\sim r^n$ for $n < 2$, and from the term $\sim r^{2n-2}$ for $n > 2$. As noted in P1, the same result holds in the gEdS models, except for one important difference: the coefficient of the leading divergence vanishes at a specific value of α . This can be seen by using the results in Table I

to infer the linear combination of these integrands which is used to obtain the one loop PS as in Eq. (24). The expansion around $(1/r) = 0$ of the resultant integrand is then

$$f_{-1}(\alpha)r^n + f_{1/2}(\alpha)r^{2n-2} + O\left[r^{n-2}, r^{2n-4}\right] \quad (32)$$

with the former giving the leading term for $n < 2$ and the latter for $n > 2$, and where

$$f_{-1}(\alpha) = \frac{7 - 14\alpha - 176\alpha^2}{15(1 + 6\alpha)(1 + 8\alpha)}, \quad (33)$$

$$f_{1/2}(\alpha) = \frac{7 + 36\alpha + 92\alpha^2}{30(1 + 6\alpha)^2}. \quad (34)$$

The indices of the functions f have been chosen to indicate the value of n at which the corresponding terms lead to ultraviolet divergence of c . As noted in P1 the function f_{-1} crosses zero at $\alpha = \alpha_c$, where

$$\alpha_c = 0.1635 \dots \quad (35)$$

while $f_{1/2}$ is always non-zero and of the same sign as in the case $\alpha = 1$ (see Fig. 1). Thus the leading divergence actually vanishes at this specific value α_c , and one loop PT gives in this case a well-defined (i.e. finite) prediction up to $n = 1/2$. The two leading terms in the expansion of the integrand in c about $(1/r) = 0$ are then given by

$$f_1(\alpha_c)r^{n-2} + f_{1/2}(\alpha_c)r^{2n-2} + O\left[r^{n-4}, r^{2n-4}\right] \quad (36)$$

where

$$f_1(\alpha) = \frac{4(1 + 2\alpha)(8\alpha - 1)}{35(1 + 6\alpha)(1 + 8\alpha)} \quad (37)$$

For $n < 0$ the first term is the leading one while for $n > 0$ it is the latter.

We will return to discuss these behaviours in more detail in Section IV below, in which we consider the regularisation of ultraviolet divergences in these models. Until then we lay aside the consideration of these divergences, deriving exact one loop results for the ultraviolet convergent regime (for any α i.e. for $n < -1$). We report our numerical tests of these results, in the still more restricted regime where they appear to be very insensitive to (finite) contributions from ultraviolet scales.

D. Exact results for PS ($-3 < n < -1$)

To obtain an analytical expression for the one-loop corrections in the range where there are the infrared divergences cancel out and there are no ultraviolet divergences, i.e. for $-3 < n < -1$, it is convenient to use dimensional regularization to treat the infrared divergences in the individual contributing terms (as in [5, 40]). To do so, it is convenient to work directly with the initial unsimplified expressions for P_{13} and P_{22} as in Eqs. (6) and (7) where P_L is a simple power-law (without cut-offs). Replacing the integrations $\int d^3q$ by $\int d^d q$ we obtain

$$P_{22}(k, a) = A^2 a^{4\alpha} \int \frac{d^d \mathbf{q}}{(2\pi)^3} q^n 2|\mathbf{k} - \mathbf{q}|^n |F_2^{(s)}(\mathbf{k} - \mathbf{q}, \mathbf{q})|^2, \quad (38)$$

$$P_{13}(k, a) = A^2 a^{4\alpha} \int \frac{d^d \mathbf{q}}{(2\pi)^3} 3q^n k^n F_3^{(s)}(\mathbf{k}, \mathbf{q}, -\mathbf{q}). \quad (39)$$

To integrate Eqs. (38) and (39) we use the formula (see the appendix in [40]) as below

$$\begin{aligned} & \int \frac{d^d \mathbf{q}}{(q^2)^{\nu_1} [(\mathbf{k} - \mathbf{q})^2]^{\nu_2}} \\ &= \frac{\Gamma(d/2 - \nu_1)\Gamma(d/2 - \nu_2)\Gamma(\nu_1 + \nu_2 - d/2)}{\Gamma(\nu_1)\Gamma(\nu_2)\Gamma(d - \nu_1 - \nu_2)} \\ & \quad \times \pi^{d/2} k^{d-2\nu_1-2\nu_2}. \end{aligned} \quad (40)$$

together with relation

$$\mathbf{k} \cdot \mathbf{q} = \pm \frac{1}{2}(k^2 + q^2 - |\mathbf{k} \mp \mathbf{q}|^2). \quad (41)$$

This leads directly to the following expressions:

$$\begin{aligned} (\hat{M}_0 + \hat{N}_0) &= \frac{2^{-(n+5)}\pi(n^2 + 2)\Gamma(\frac{1}{2} - n)\Gamma(\frac{n+1}{2})}{\Gamma(2 - \frac{n}{2})^2\Gamma(\frac{n+2}{2})}, \\ \hat{M}_1 &= -\frac{2^{-(n+2)}\pi\Gamma(\frac{1}{2} - n)\Gamma(\frac{n+3}{2})}{\Gamma(2 - \frac{n}{2})^2\Gamma(\frac{n+2}{2})}, \\ \hat{M}_2 &= \frac{2^{-(n+2)}\pi\Gamma(\frac{1}{2} - n)\Gamma(\frac{n+3}{2})}{\Gamma(2 - \frac{n}{2})^2\Gamma(\frac{n+4}{2})}, \\ \hat{N}_1 &= \frac{3\pi^2 \csc\left(\frac{(n+3)\pi}{2}\right)}{8\Gamma(1 - \frac{n}{2})\Gamma(\frac{n}{2} + 4)}, \\ \hat{N}_2 &= -\frac{3\pi^2 \csc\left(\frac{(n+3)\pi}{2}\right)}{16\Gamma(2 - \frac{n}{2})\Gamma(\frac{n}{2} + 3)} \end{aligned} \quad (42)$$

from which it follows that

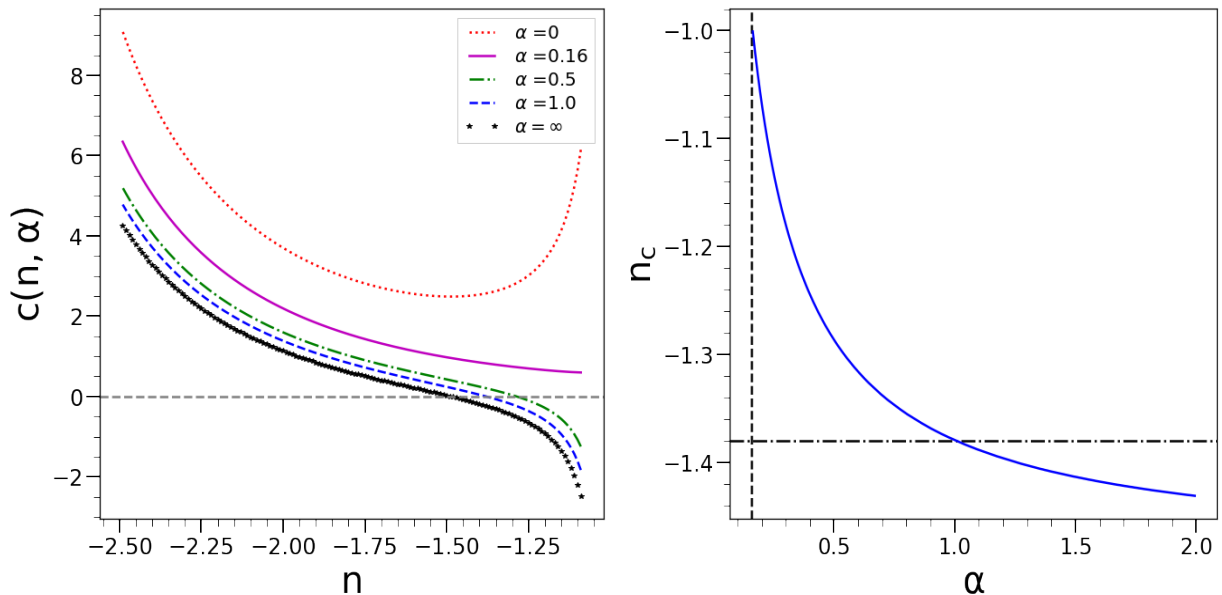


FIG. 2. Left panel: coefficient c characterising the one-loop correction to the PS in standard perturbation theory, as a function of n in the range $n < -1$ where the result is finite, for different values of α . Right panel: the critical value $n = n_c$ at which the one-loop correction to the PS changes sign, as a function of α . The black dash-dotted horizontal line corresponds to standard EdS for which $n \approx -1.38$, and the black dashed vertical lines indicate the critical value $\alpha_c \approx 0.16$ below which c is always positive.

$$\begin{aligned}
 c(n, \alpha) = & \frac{2^{-(n+2)} \pi \Gamma(\frac{1}{2} - n) \Gamma(\frac{n+3}{2})}{\Gamma(2 - \frac{n}{2})^2 \Gamma(\frac{n+2}{2})} \left[\frac{(n^2 + 2)}{4(n+1)} + \left(\frac{1+4\alpha}{1+6\alpha} \right) \left\{ 1 + \left(\frac{1+4\alpha}{1+6\alpha} \right) \frac{1}{n+2} \right\} \right] \\
 & + \left(\frac{1+2\alpha}{1+8\alpha} \right) \frac{3\pi}{8} \left(\frac{\Gamma(\frac{n+3}{2}) \Gamma(-\frac{n+1}{2})}{\Gamma(1 - \frac{n}{2}) \Gamma(\frac{n}{2} + 3)} \right) \left[\frac{2}{n+6} - \left(\frac{2\alpha}{1+6\alpha} \right) \frac{1}{2-n} \right].
 \end{aligned} \tag{43}$$

Setting $\alpha = 1$ in the individual expressions for P_{13} and P_{22} used to derive Eq. (43), we have checked that we recover identical expressions to those in [5] and [40].¹

A further check on the correctness of the expression Eq. (43) is obtained by comparing with the exact result for the case $n = -2$ which, as detailed further below in Section IV, can be obtained directly using the expressions in Eq. (26) as

$$c(n = -2, \alpha) = \frac{3\pi^2(4\alpha + 1)(22\alpha^2 + 10\alpha + 1)}{8(6\alpha + 1)^2(8\alpha + 1)} \tag{44}$$

The left panel of Fig. 2 shows $c(n, \alpha)$ as a function of n for different chosen values of α , including the canonical $\alpha = 1$ case. Compared to the latter, the most evident

qualitative change as α varies is that the zero crossing of c , which is at $n = n_c \approx -1.38$ for $\alpha = 1$, not only increases towards $n = -1$ as α decreases but actually ceases to exist at a certain critical value of α . The right panel of Fig. 2 shows the quantitative behaviour of n_c as a function of α . This critical value is none other than α_c , the positive root of the function f_{-1} discussed above, at which the leading divergence changes sign. Indeed we can see this also by expanding our expression Eq. (43) around $n \rightarrow -1$, where it has a simple pole, which gives

$$\begin{aligned}
 c(n = -1 + \xi, \alpha) = & -\frac{(7 - 14\alpha - 176\alpha^2)}{15(6\alpha + 1)(8\alpha + 1)\xi} \\
 & + \frac{4(2\alpha + 1)(4\alpha + 1)}{9(6\alpha + 1)^2} + \dots
 \end{aligned} \tag{45}$$

We note also that, other than very close to the divergence, c is a very slowly varying function of α in the range of α which is relevant to current standard type models, for which the logarithmic linear growth rate varies between $\alpha = 1$ (and high redshift) and $\alpha \sim 0.5$. As discussed in P1, the correction to the one loop PS relative

¹ As noted in [5], there is a sign error in one term in the expression for the fourth term of P_{22} given in [40]. The latter reference also defines a coefficient labelled α_δ analogous to our c , but differing by a factor, with $\alpha_\delta = \frac{2}{\Gamma(\frac{n+3}{2})} c$.

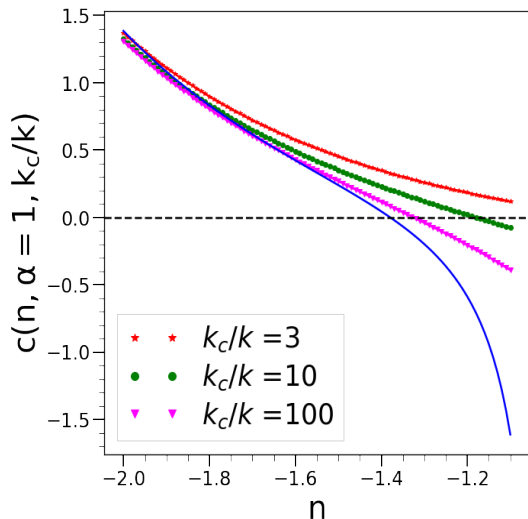


FIG. 3. Numerically evaluated $c(n, \alpha = 1, k_c/k)$ for different indicated values of the cut-off k_c , as a function of n . Also shown is the exact result (solid line) obtained using dimensional regularisation.

to the EdS value in these models can be well approximated (to about 20 – 25%) by calculating in a gEdS model with an effective value at $z = 0$ of $\alpha \sim 0.9$ (which represents an appropriately averaged growth rate over the cosmological evolution).

III. NUMERICAL TESTS OF PREDICTED α -DEPENDENCE (FOR $n = -2$)

In this section we compare the results of numerical simulations with the analytical result given by Eq. (43). While it is potentially of interest to consider a wide range of different n and α , we limit ourselves here to probing the α -dependence (which is the novelty of our analysis) of the result for n in the regime where we expect that this result may actually provide a good approximation i.e. where the ultraviolet sensitivity of the result is weak, for n well below -1 . To quantify this a little more we show, in Fig. 3, the results of a determination of $c(n, \alpha, k_c/k)$ by direct numerical integration for the different indicated values of the cut-off k_c/k . The ultra-violet sensitivity as expected diminishes markedly as n decreases. In the left panel of Fig. 2 we see, on the other hand, that the α -dependence remains quite uniform for $n < -1.5$. If n decreases too close to $n = -3$, however, the dynamical range of a simulation due to the finite simulation box size will become very limited. We thus consider the value $n = -2$. Figure 4 shows, for this value of n , the predicted difference as a function of α between the coefficient c and its value for $\alpha = 1$. Given that the modification of the PS is proportional to c multiplied by $\Delta_L^2(k)$, and that the one-loop calculation is expected to be valid only for small values of the latter, it is evidently of interest to simulate

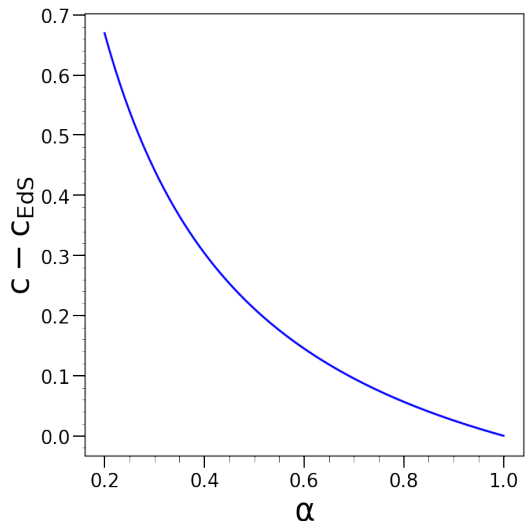


FIG. 4. Difference between the coefficient $c(n = -2, \alpha)$ and its value in the standard EdS model $c_{\text{EdS}} = c(n = -2, \alpha = 1)$, for α in the range explored by our suite of simulations. Note that it is this quantity multiplied by Δ_L^2 which gives the fractional change in the predicted PS, and one loop PT is expected only to apply for $\Delta_L^2 \ll 1$. At $\Delta_L^2 \sim 0.1$ the predicted maximal change in power, for $\alpha = 0.25$, is thus of order of 5%. This can be compared with the much smaller changes in standard (LCDM-like) models, of order 0.5% at $z = 0$ (see P1 and [42–44])

smaller values of α for which the difference in power is amplified. We consider here simulations with $N = 256^3$ particles, and the values $\alpha = 1.00, 0.7, 0.5, 0.33, 0.25$. The lower limit $\alpha = 0.25$ is imposed, as we will explain further below, because the numerical cost of the simulations increases strongly as α decreases. Nevertheless this value is sufficient to give predicted changes in the power of order 5% for $\Delta_L^2 = 0.1$, much greater (and therefore much easier to measure numerically) than the predicted changes of $\sim 0.5\%$ in standard (LCDM-like) models (see [42–44]). As discussed in P1, the latter can be well approximated by using a gEdS model with $\alpha \approx 0.9$.

A. Simulation method

Our numerical results here have been obtained using N -body simulations performed with an appropriately modified version of the GADGET2 code [45] as described in detail in [46], and further in [47]. Indeed the class of scale-free models we are considering cannot be simulated by the standard version of GADGET2 code, which allows only expanding backgrounds specified by the standard cosmological parameters. The gEdS cosmology has been implemented instead by modifying the module of the GADGET2 code which allows simulation also of a *static* universe (i.e. of an infinite periodic system without expansion). The usual equations solved in N -body simulations for particles in an expanding background are

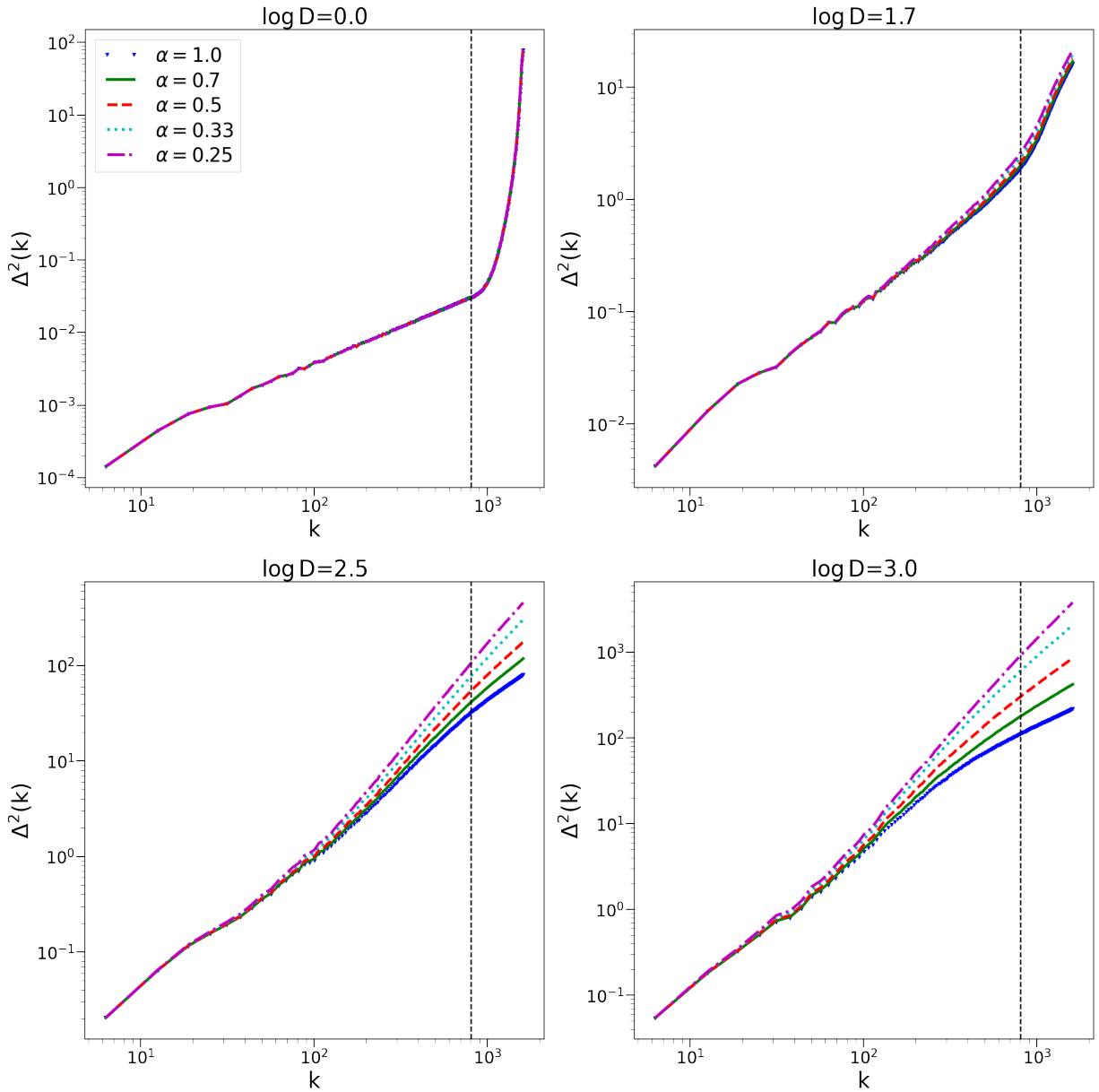


FIG. 5. Dimensionless PS measured in our suite of five simulations, with the indicated values of α , as a function of k (in units in which the boxsize $L = 1$). The first panel is the initial configuration (with identical power in each simulation) and the other three progressively more evolved snapshots.

given in comoving coordinates \mathbf{x} as

$$\frac{d^2 \mathbf{x}_i}{dt^2} + 2H \frac{d\mathbf{x}_i}{dt} = \frac{1}{a^3} \mathbf{F}_i \quad (46)$$

where the gravitational force is

$$\mathbf{F}_i = -Gm \sum_{j \neq i}^P \frac{\mathbf{x}_i - \mathbf{x}_j}{|\mathbf{x}_i - \mathbf{x}_j|^3} W_\varepsilon(|\mathbf{x}_i - \mathbf{x}_j|). \quad (47)$$

with W_ε a function that smooths the singularity of the Newtonian force at zero separation, at a characteristic scale ε , and the ‘‘P’’ in the sum indicates that there is a

sum over the copies of the periodic system. As discussed in further detail in [46], these equations can be recast, by the simple change of time coordinate $\tau = \int dt a^{-3/2}$, as

$$\frac{d^2 \mathbf{x}_i}{d\tau^2} + \Gamma \frac{d\mathbf{x}_i}{d\tau} = \mathbf{F}_i, \quad (48)$$

where

$$\Gamma = \frac{1}{2} a^{3/2} H = \frac{1}{2} a^{-1} \frac{da}{d\tau}. \quad (49)$$

Thus the equations of motion are just those of self-gravitating particles in a non-expanding system subject

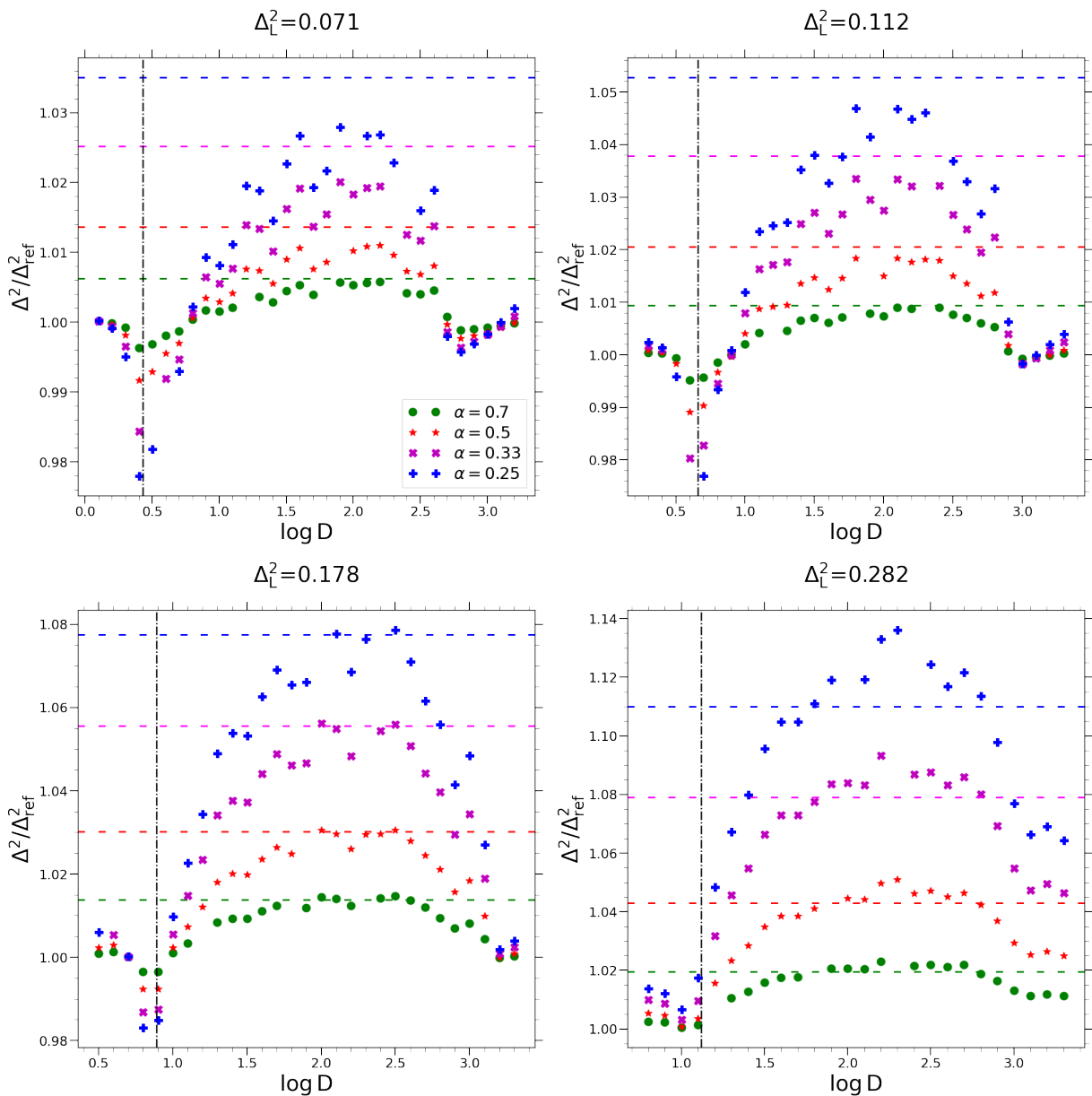


FIG. 6. Ratios of PS measured in the four simulations with $\alpha < 1$ to that measured in the standard EdS ($\alpha = 1$) simulation, as a function of time parametrized as $\log D$. Each plot corresponds to the indicated chosen value of the theoretical input dimensionless PS Δ_L^2 . Self-similar behaviour (i.e. a result independent of the scales introduced by the N -body simulation) corresponds to a constant value. The different horizontal lines correspond to the (self-similar) ratios predicted by one loop standard perturbation theory. The vertical line on each plot indicates the time at which $k = k_N$, the Nyquist wavenumber of the particle grid.

to a simple fluid damping. The family of $gEdS$ cosmologies corresponds to models given by a constant value of Γ , with

$$\Gamma = \kappa \sqrt{2\pi G \rho_0 / 3} \quad (50)$$

where ρ_0 is the mean mass density at some chosen reference time. The static universe module of GADGET2 has thus been modified to include this constant fluid-damping term, keeping the original “Kick-Drift-Kick” structure of its leap-frog algorithm and modifying appropriately the

“Kick” and “Drift” operations. The structure of the code is otherwise unchanged. Further details and various tests of the modified code have been described in [46], in particular tests of energy conservation (using the so-called Layzer-Irvine equations) as well as a direct comparison showing excellent agreement between simulations of the standard EdS (i.e. $\alpha = 1$) model using the existing GADGET2 expanding universe module and the new modified static universe module.

To generate initial conditions we use the canonical

method, applying displacements to the simulation particles initially placed on a perfect lattice, and ascribing corresponding initial velocities, as prescribed by the Zeldovich approximation, for a random realization of a Gaussian fluctuation field with the chosen input PS (for more details see e.g. [48] and [49]). At the starting time, a_0 , the initial amplitude of the PS has been set using the specific choice (following the criteria of [33, 50])

$$\Delta_L^2(k_N, a_0) = 0.03 \quad (51)$$

where k_N is the Nyquist frequency of the initial particle grid. We use the same realization of the initial density field in all five simulations. The initial displacements are thus identical in the five simulations, and the initial velocities simply rescaled appropriately for each α (since the Zeldovich displacement is proportional to D).

Outputs of the simulations have been saved, starting from the initial time, at times defined by

$$t_s = \log D(a) = 0.1 s \quad (52)$$

where $D(a)$ is the linear growth factor, defined so that $D(a_0) = 1$, and $s = 0, 1, 2 \dots 33$. Thus the predicted linear power spectrum in each simulation is identical at each output, and the final output, at $a = a_f$, corresponds to an amplitude $\Delta_L^2(k_b, a_0) = e^{6.6} 0.03 / 256 \approx 0.17$ at the fundamental mode $k_b = 2\pi/L$ of the periodic box. As we will see below by this time the finite box size corrections are very dominant over the very small effects we are seeking to measure (at the few percent levels).

To calculate the power spectrum based on data from N-body simulations, we have used the publicly available POWMES code [51] with the size of FFT grid equal to 512^3 (compared to the 256^3 initial particle grid) and without any “foldings”. This is quite sufficient resolution for the analysis here, focussing on smaller k .

B. Results

Figure 5 shows the dimensionless PS measured in the five simulations, at the starting time and at three subsequent times. We observe a qualitative behaviour in line with Fig. 4: as α decreases the non-linear power increases. However this is in fact visibly the case in this plot only starting from Δ^2 approaching unity, where we do not expect perturbation theory to apply. Indeed as we have discussed, Fig. 4 implies changes to the non-linear power of at most about ten percent. The origin of the amplification of the highly non-linear power we observe in this plot — and more particularly the steepening of its slope as a function of α has been discussed at length in [26]. Here we focus instead on the perturbative regime.

We also see in Fig. 5 the visible effects of finite mode sampling on the small k modes (i.e. small Δ_L^2) which are relevant for the regime we are interested in: indeed there is clearly a significant offset in this regime between the theoretical linear power spectrum $\Delta^2(k)$ and the actual

initial power $\Delta_{sim}^2(k)$ in the realization of the initial conditions in the periodic box. Thus we expect that a comparison of the observed power with the theoretical prediction can be accurate at best up to a systematic error of order $\delta = (\Delta^2(k) / \Delta_{sim}^2(k)) - 1$, while if we consider the measured *ratio* of the power between two simulations we can expect accuracy instead of $\delta \times [c(n, \alpha) - c(n, \alpha = 1)]$. In order to measure the very small effects predicted, we therefore consider this relative measurement, using (arbitrarily) $\alpha = 1$ as our reference.

Figure 6 shows illustrative examples of our results for the relative power in the four simulations with $\alpha < 1$ with that in the standard EdS case. Following the analysis method developed in [24, 25], each panel is for a different bin of Δ_L^2 (corresponding to a fixed bin of rescaled wavenumber k/k_{NL}), and shows the ratios measured in the different snapshots. The indicated values of Δ_L^2 correspond to those calculated for the theoretical input PS spectrum at the geometric centre (in k) of the bins, which are equally spaced in log space with $\Delta \log_{10} k = 0.1$. The measured power spectrum is self-similar if and only if it is a function of $\Delta_L^2(k)$ only i.e. if it is constant in this plot. The ratios of the measured (self-similar) power predicted by eq. (43) for each value of α , is indicated by an horizontal line².

As discussed in (much larger, but standard EdS) simulations [25] what we observe in these plots is a finite range of time in which each rescaled k/k_{NL} approximates self-similarity, with deviations at early times due to ultraviolet cut-offs (grid spacing, force smoothing) and at late times due to the infrared cut-off given by the box-size. Indeed as we move from left to right in each plot, the associated comoving k increases, with the vertical line in the plot indicating the time at which k corresponds to the Nyquist wavenumber of the initial grid. The effects of the finite box size are clearly visible in all plots as a suppression of the relative power in the more evolved snapshots, which sets in at later times in the successive plots (as Δ_L^2 , and therefore the associated k increases). Indeed in the first plot, corresponding to the smallest k at a fixed time, this break happens so early that most of the plots show no clearly converged regime. On the other hand all the other plots show, to differing degrees of accuracy, clear evidence for a converged self-similar behaviour. In all these cases this value agrees well with the predicted theoretical values. Further this agreement is best in the regime where we expect perturbation theory to be most accurate i.e. where these perturbative corrections are the smallest. We conclude that the α -dependence of the power observed in our simulations are apparently in good agreement with the one-loop PT predictions.

² The finite size of the bins has also been taken into account in this latter calculation but only very marginally modifies the result.

IV. α DEPENDENCE OF UV DIVERGENCES AND THEIR REGULATION

General considerations (see e.g. [28]) lead one to expect that non-linear cosmological clustering should be ultra-violet insensitive for power-law initial conditions $P(k) \propto k^n$ provided $n < 4$. For scale-free models, with an EdS expansion law, such cut-off independence implies self-similarity. Numerous numerical studies confirm that such self-similarity is indeed observed, with different authors exploring different ranges of n , up to $n = 2$ (see e.g. [26, 29–38, 52]). The ultra-violet divergences which render the predictions of SPT undefined as n approaches -1 from below are a priori therefore unphysical. The PS of standard cosmologies, however, at large k has a behaviour (typically $\sim k^{-3} \log k$) which leads to finite SPT predictions. Nevertheless there is also a region where the effective logarithmic slope of the PS corresponds to that of the ultraviolet divergent region, and one expects then that the associated unphysical divergences lead to inaccuracies of the predictions of SPT. In the last number of years there has been much interest and work on the so-called effective field theory (EFT) approach to the regulation of this ultraviolet divergences (see e.g. [2, 3, 5, 7–18, 20, 21]). This theory provides a systematic approach to the problem directly inspired from that used in high energy physics.

Without employing the full machinery of EFT, we can recover very simply its results for the class of model we are considering. To do so we impose a finite ultraviolet cut-off in the PS (i.e. we take k_c to be finite) above, and then consider how k_c can scale with k in a manner compatible with self-similarity.

For $n \geq -1$, an analytical expression for $c(n, \alpha, k_c/k)$ (with k_c/k finite) can be found for integer values of n . To do so, as shown e.g. by [39], one can conveniently rewrite the \hat{M}_i double integrals by breaking up the integration range as

$$\begin{aligned} \int_{\epsilon}^{1/\omega} dr \int_{\mu_{min}}^{\mu_{max}} d\mu &= \int_{\epsilon}^{1-\epsilon} dr \int_{-1}^1 d\mu \\ &+ \int_{1+\epsilon}^{(1/\omega)-1} dr \int_{-1}^1 d\mu \\ &+ \int_{1-\epsilon}^{1+\epsilon} dr \int_{-1}^{(1+r^2-\epsilon^2)/2r} d\mu \\ &+ \int_{(1/\omega)-1}^{1/\omega} dr \int_{(1+r^2-\omega^{-2})/2r}^1 d\mu, \end{aligned}$$

where $\epsilon = (\epsilon/k)$ and $\omega = (k/k_c)$. For the \hat{N}_i integrals we simply divide the integration range over r into ϵ to 1 and from 1 to $1/\omega$. For each of the resulting integrals an explicit analytic expression can be obtained (using Mathematica [53]), and written as a series expansion about $\epsilon = 0$ or $\omega = 0$, with poles associated with the divergences we have analysed. As previously discussed the divergences as $\epsilon \rightarrow 0$ in \hat{M}_0 and \hat{N}_0 cancel for $n > -3$. The

results for the individual integrals, \hat{M}_i and \hat{N}_i , are shown in Table II and the resulting expressions for $c(n, \alpha, k_c/k)$ in Table III. In each case we have included terms in the expansion around $\omega = 0$ and $\epsilon = 0$ which do not vanish when the latter goes to zero. We note that the terms which diverge as k_c/k are in agreement with the results for the leading ultraviolet divergences given in Section II, with the leading divergence $\sim k_c^{n+1}$ and the following one at $\sim k_c^{2n-1}$. Further in the expressions for c we recover exactly the factors proportional to the α -dependent coefficients f_{-1} , $f_{1/2}$ and f_1 given in Eqs. (33)-(34) and (37).

In order to respect self-similarity it is sufficient to choose a regularization k_c/k which is assumed to be some function of $\Delta_L^2(k)$. The simplest and natural choice is to take

$$k_c \propto k_{NL} \quad (53)$$

i.e. to assume that the effective cut-off in the one-loop integrals is set by the non-linearity scale. Using this prescription we write the regularized result first as

$$\begin{aligned} \tilde{c}_{reg}(n, \alpha, \frac{k_{NL}}{k}) &= c(n, \alpha, \frac{k_c}{k} = \gamma \frac{k_{NL}}{k}) \\ &= \lim_{\lambda \rightarrow \infty} \left[c(n, \alpha, \frac{k_c}{k} = \lambda) + \Delta c(n, \alpha, \gamma, \lambda) \right] \end{aligned}$$

where

$$\Delta c = c(n, \alpha, \gamma \frac{k_{NL}}{k}) - c(n, \alpha, \lambda). \quad (54)$$

Assuming that $\gamma \frac{k_{NL}}{k}$ and λ are large, we can use the results of our analysis of the ultraviolet divergences in Section II C to obtain the expansion of Δc :

$$\begin{aligned} \Delta c &= \frac{f_{-1}}{n+1}(\alpha) [\gamma^{n+1} (\frac{k_{NL}}{k})^{n+1} - \lambda^{n+1}] \\ &+ \frac{f_{1/2}}{2n-1}(\alpha) [\gamma^{2n-1} (\frac{k_{NL}}{k})^{2n-1} - \lambda^{2n-1}] \\ &+ \frac{f_1}{n-1}(\alpha) [\gamma^{n-1} (\frac{k_{NL}}{k})^{n-1} - \lambda^{n-1}] + \dots \end{aligned} \quad (55)$$

for any n other than the specific values $n = -1, 1/2, 1, \dots$, where the power-law functions are replaced by logarithms. For the sake of brevity, we will not give results for these special cases explicitly here. Using these expressions the regularized one-loop result can now be written as

$$\begin{aligned} \Delta_{1-loop, reg}^2(k) &= \Delta_L^2(k) \left[1 + c_{reg}(n, \alpha) \Delta_L^2(k) \right. \\ &+ f_{-1}(\alpha) \frac{\gamma^{n+1}}{n+1} (\Delta_L^2(k))^{\frac{2}{3+n}} \\ &+ f_{1/2}(\alpha) \frac{\gamma^{2n-1}}{2n-1} (\Delta_L^2(k))^{\frac{4-n}{3+n}} \\ &\left. + f_1(\alpha) \frac{\gamma^{n-1}}{n-1} (\Delta_L^2(k))^{\frac{4-n}{3+n}} \right] \end{aligned} \quad (56)$$

TABLE II. Analytical expressions for the six integrals, \hat{M}_i and \hat{N}_i (for $i = 0, 1, 2$), for $n = 1$, $n = 0$, $n = -1$ and $n = -2$, up to linear order in k/k_c and in the limit $\epsilon = 0$.

\hat{M}_i, \hat{N}_i	n=1	n=0	n=-1	n=-2
\hat{M}_0	$\frac{1}{2} \left(\frac{k_c}{k}\right) - \frac{7}{8}$	$\frac{\pi^2}{16}$	$\frac{1}{3} \log\left(\frac{k}{\epsilon}\right)$	$\frac{k}{3\epsilon}$
\hat{M}_1	$-\frac{4}{3} \left(\frac{k_c}{k}\right) + \frac{9}{4}$	$-\frac{\pi^2}{8}$	$-\frac{4}{9}$	0
\hat{M}_2	$\frac{16}{15} \left(\frac{k_c}{k}\right) - \frac{3}{2}$	$\frac{\pi^2}{8}$	$\frac{8}{9}$	$\frac{3\pi^2}{16}$
\hat{N}_0	$-\frac{1}{6} \left(\frac{k_c^2}{k^2}\right)$	$-\frac{1}{3} \left(\frac{k_c}{k}\right)$	$\frac{1}{3} \log\left(\frac{\epsilon}{k_c}\right)$	$-\frac{k}{3\epsilon}$
\hat{N}_1	$\frac{2}{5} \left(\frac{k_c^2}{k^2}\right) + \frac{4}{35} \log\left(\frac{4k}{k_c}\right) - \frac{958}{1225}$	$\frac{4}{5} \left(\frac{k_c}{k}\right) - \frac{\pi^2}{16}$	$-\frac{4}{5} \log\left(\frac{k}{k_c}\right) + \frac{32}{75}$	$\frac{3\pi^2}{16}$
\hat{N}_2	$-\frac{2}{3} \left(\frac{k_c^2}{k^2}\right) - \frac{4}{5} \log\left(\frac{4k}{k_c}\right) + \frac{142}{75}$	$-\frac{4}{3} \left(\frac{k_c}{k}\right) + \frac{3\pi^2}{16}$	$\frac{4}{3} \log\left(\frac{k}{k_c}\right)$	$-\frac{3\pi^2}{16}$

TABLE III. Analytical expressions for the one-loop coefficients $c(n, \alpha, k_c/k)$ for $n = 1$, $n = 0$, $n = -1$ and $n = -2$ up to linear order in k/k_c and in the limit $\epsilon = 0$.

n	$c(n, \alpha, k_c/k)$
1	$\frac{(7-14\alpha-176\alpha^2)}{30(6\alpha+1)(8\alpha+1)} \left(\frac{k_c}{k}\right)^2 + \frac{(7+36\alpha+92\alpha^2)}{30(1+6\alpha)^2} \frac{k_c}{k} + \frac{4(2\alpha+1)(8\alpha-1) \log\left(\frac{k_c}{4k}\right)}{35(6\alpha+1)(8\alpha+1)} - \frac{4\alpha(\alpha(168072\alpha+133249)+59990)+26667}{29400(6\alpha+1)^2(8\alpha+1)}$
0	$\frac{(7-14\alpha-176\alpha^2)}{15(6\alpha+1)(8\alpha+1)} \frac{k_c}{k} + \frac{\pi^2\alpha(4\alpha+1)(5\alpha+1)}{2(6\alpha+1)^2(8\alpha+1)}$
-1	$\frac{(7-14\alpha-176\alpha^2)}{15(6\alpha+1)(8\alpha+1)} \ln \frac{k_c}{k} + \frac{4(2\alpha+1)(32\alpha+7)(52\alpha+7)}{225(6\alpha+1)^2(8\alpha+1)}$
-2	$\frac{3\pi^2(4\alpha+1)(2\alpha(11\alpha+5)+1)}{8(6\alpha+1)^2(8\alpha+1)}$

where

$$c_{reg} = \lim_{\lambda \rightarrow \infty} \left[c(n, \alpha, \lambda) - f_{-1}(\alpha) \frac{\lambda^{n+1}}{n+1} - f_{1/2}(\alpha) \frac{\lambda^{2n-1}}{2n-1} - f_1(\alpha) \frac{\lambda^{n-1}}{n-1} + \dots \right] \quad (57)$$

This result is almost exactly equivalent to that obtained in EFT, corresponding to the addition of the counter-terms

$$c_1 k^2 P_L(k) + c_2 k^4 + c_3 k^4 P_L(k) \quad (58)$$

where we have, additionally, that

$$\begin{aligned} c_1 &= (2\pi^2)^{\frac{2}{3+n}} f_{-1}(\alpha) \frac{\gamma^{n+1}}{n+1} \\ c_2 &= (2\pi^2)^{\frac{4-n}{n+3}} f_{1/2}(\alpha) \frac{\gamma^{2n-1}}{2n-1} \\ c_3 &= (2\pi^2)^{\frac{4}{n+3}} f_1(\alpha) \frac{\gamma^{n-1}}{n-1} \end{aligned} \quad (59)$$

where $\gamma = k_{NL}/k_c$, a positive constant which may also depend also on n and α . Usually only the first two terms are included, as they represent the leading corrections (the first term for $n < 2$ and the second for $n > 2$). As we have discussed, this is sufficient here also other than when $\alpha = \alpha_c$. In this case we have $c_1 = 0$, which makes the third term the leading EFT correction for $n < 0$. Correspondingly the expression for c_{reg} is just the unregularized result $c_\infty(n, \alpha)$ for $n < -1$, and then regularized

appropriately for $n \geq -1$, except again for α_c where the unregularized result remains valid up to $n = 1/2$.

The ultraviolet regularized one loop result for the family of generalized scale-free models thus gives a very specific prediction that can be used in principle to test this regularisation framework: the sign of the correction to the raw (unregularized) one loop result should depend on α as given by $f_{-1}(\alpha)$, and in particular at $\alpha = \alpha_c$ it vanishes so that, in this case, the raw (unregularized) one-loop result gives a well-defined finite prediction up to $n = 1/2$. A suite of simulations for n around -1 like those reported above for the case $n = -2$, but extending to smaller α , would allow us to probe this regime. Simulating such small values of α is however more challenging numerically, because we have $k_{NL} \propto a^{\frac{2\alpha}{3+n}}$ and therefore the ratio of the final to the initial scale factors of a simulation is given by

$$\frac{a_f}{a_i} = \left(\frac{k_{NL}(a_i)}{k_{NL}(a_f)} \right)^{\frac{3+n}{2\alpha}} \quad (60)$$

In order to make use of self-similarity in order to establish accurately converged values of the PS, we need the factor $\frac{k_{NL}(a_i)}{k_{NL}(a_f)}$ to be reasonably large (at least a decade). For $n = -1$ and $\alpha \approx 0.16$ the exponent is three times larger than it was for the smallest value α we reported above for $n = -2$. This means that, for a given $\frac{k_{NL}(a_i)}{k_{NL}(a_f)}$, the non-linear structures formed will become relatively much denser as n increases and/or α decreases. This can in principle be remedied by using a sufficiently large gravitational smoothing ϵ , but in this case one must control carefully that its effects do not propagate to the interme-

diate (weakly non-linear) scales we are interested in for comparison with perturbation theory.

V. DISCUSSION AND CONCLUSIONS

We have studied the PS calculated at one loop in standard Eulerian perturbation theory for the family of generalized scale-free cosmologies, characterized by initial Gaussian fluctuations with a pure power law PS and an EdS expansion driven by clustering pressureless matter as well as a smooth pressureless component. We have thus generalized existing analytic results for the standard EdS case [39, 40] to this one-parameter family, with the corresponding analytic expressions now becoming functions not just of the power law exponent n but also of the logarithmic growth rate α in the model. While in the standard case $\alpha = 1$, the parameter α can vary in the range $0 < \alpha \leq \infty$, with the lower limit corresponding to an infinite Hubble rate and the upper limit to a static universe.

While these models are idealized and very different from typical standard cosmological models, they provide a simple framework in which to test cosmological perturbation theory. Specifically they are evidently designed to probe the cosmology dependence, and indeed we have seen here that, by exploiting self-similarity, it is possible with even quite small N -body simulations to test and

validate its predictions to a high degree of accuracy. To our knowledge, this is the first time that the predictions of perturbation theory for dependence on the growth rate of fluctuations have been tested numerically.

Further we have argued that these models are an interesting tool to probe the regularisation of PT, and specifically the EFT approach to this problem. This is the case because the associated divergences, and thus their regularisation, have non-trivial dependences on the parameter α . In particular this leads to the vanishing of the leading correction in EFT at a specific value of α . As we have discussed the regime of n and small α of relevance to test these predictions poses some numerical challenges beyond that which was needed for the simulations we have reported here. This is the subject of ongoing study.

ACKNOWLEDGMENTS

We thank Bruno Marcos for his collaboration in the modification of GADGET2 in [26], and Sara Maleubre for useful discussions on the analysis of the PS in scale-free simulations. A.P. is supported by Indonesia Endowment Fund for Education (LPDP). Numerical simulations have been performed on a cluster at MeSU hosted at Sorbonne Université.

-
- [1] F. Bernardeau, S. Colombi, E. Gaztañaga, and R. Scoccimarro, Phys. Rept. **367**, 1 (2002), arXiv:astro-ph/0112551 [astro-ph].
 - [2] D. Baumann, A. Nicolis, L. Senatore, and M. Zaldarriaga, JCAP **2012** (7), 051, arXiv:1004.2488 [astro-ph.CO].
 - [3] J. J. M. Carrasco, M. P. Hertzberg, and L. Senatore, JHEP **2012**, 82, arXiv:1206.2926 [astro-ph.CO].
 - [4] A. Taruya, F. Bernardeau, T. Nishimichi, and S. Codis, Phys. Rev. D **86**, 103528 (2012), arXiv:1208.1191 [astro-ph.CO].
 - [5] E. Pajer and M. Zaldarriaga, JCAP **2013** (8), 037, arXiv:1301.7182 [astro-ph.CO].
 - [6] D. Blas, M. Garny, and T. Konstandin, JCAP **2014** (1), 010, arXiv:1309.3308 [astro-ph.CO].
 - [7] M. P. Hertzberg, Phys. Rev. D **89**, 043521 (2014), arXiv:1208.0839 [astro-ph.CO].
 - [8] L. Mercolli and E. Pajer, JCAP **2014** (3), 006, arXiv:1307.3220 [astro-ph.CO].
 - [9] R. A. Porto, L. Senatore, and M. Zaldarriaga, JCAP **2014** (5), 022, arXiv:1311.2168 [astro-ph.CO].
 - [10] S. M. Carroll, S. Leichenauer, and J. Pollack, Phys. Rev. D **90**, 023518 (2014), arXiv:1310.2920 [hep-th].
 - [11] J. J. M. Carrasco, S. Foreman, D. Green, and L. Senatore, JCAP **2014** (7), 057, arXiv:1310.0464 [astro-ph.CO].
 - [12] J. J. M. Carrasco, S. Foreman, D. Green, and L. Senatore, JCAP **2014** (7), 056, arXiv:1304.4946 [astro-ph.CO].
 - [13] L. Senatore and M. Zaldarriaga, arXiv e-prints , arXiv:1409.1225 (2014), arXiv:1409.1225 [astro-ph.CO].
 - [14] L. Senatore and M. Zaldarriaga, JCAP **2015** (2), 013, arXiv:1404.5954 [astro-ph.CO].
 - [15] T. Baldauf, L. Mercolli, M. Mirbabayi, and E. Pajer, JCAP **2015** (5), 007, arXiv:1406.4135 [astro-ph.CO].
 - [16] Z. Vlah, M. White, and A. Aviles, JCAP **2015** (9), 014, arXiv:1506.05264 [astro-ph.CO].
 - [17] R. E. Angulo, S. Foreman, M. Schmittfull, and L. Senatore, JCAP **2015** (10), 039, arXiv:1406.4143 [astro-ph.CO].
 - [18] T. Baldauf, L. Mercolli, and M. Zaldarriaga, Phys. Rev. D **92**, 123007 (2015), arXiv:1507.02256 [astro-ph.CO].
 - [19] M. Crocce and R. Scoccimarro, Phys. Rev. D **73**, 063519 (2006), arXiv:astro-ph/0509418 [astro-ph].
 - [20] S. Foreman and L. Senatore, JCAP **2016** (4), 033, arXiv:1503.01775 [astro-ph.CO].
 - [21] T. Steele and T. Baldauf, Phys. Rev. D **103**, 023520 (2021), arXiv:2009.01200 [astro-ph.CO].
 - [22] Z. Wang, D. Jeong, A. Taruya, T. Nishimichi, and K. Osato, arXiv e-prints , arXiv:2209.00033 (2022), arXiv:2209.00033 [astro-ph.CO].
 - [23] M. Garny, D. Laxhuber, and R. Scoccimarro, Phys. Rev. D **107**, 063540 (2023), arXiv:2210.08089 [astro-ph.CO].
 - [24] M. Joyce, L. Garrison, and D. Eisenstein, Mon. Not. Roy. Astron. Soc. **501**, 5051 (2021), arXiv:2004.07256 [astro-ph.CO].
 - [25] S. Maleubre, D. Eisenstein, L. H. Garrison, and M. Joyce, Mon. Not. Roy. Astron. Soc. **512**, 1829 (2022), arXiv:2109.04397 [astro-ph.CO].
 - [26] D. Benhaiem, M. Joyce, and B. Marcos, Mon. Not. Roy.

- Astron. Soc. **443**, 2126 (2014), arXiv:1309.2753 [astro-ph.CO].
- [27] M. Joyce and A. Pohan, Phys. Rev. D (2023), arXiv:2207.04419 [astro-ph.CO].
- [28] P. J. E. Peebles, *The large-scale structure of the universe* (1980).
- [29] G. Efstathiou, C. S. Frenk, S. D. M. White, and M. Davis, Mon. Not. Roy. Astron. Soc. **235**, 715 (1988).
- [30] T. Padmanabhan, R. Cen, J. P. Ostriker, and F. J. Summers, Astrophys. J. **466**, 604 (1996), arXiv:astro-ph/9506051 [astro-ph].
- [31] S. Colombi, F. R. Bouchet, and L. Hernquist, Astrophys. J. **465**, 14 (1996), arXiv:astro-ph/9508142 [astro-ph].
- [32] B. Jain and E. Bertschinger, Astrophys. J. **456**, 43 (1996), arXiv:astro-ph/9503025 [astro-ph].
- [33] B. Jain and E. Bertschinger, Astrophys. J. **509**, 517 (1998), arXiv:astro-ph/9808314 [astro-ph].
- [34] R. E. Smith, J. A. Peacock, A. Jenkins, S. D. M. White, C. S. Frenk, F. R. Pearce, P. A. Thomas, G. Efstathiou, and H. M. P. Couchman, Mon. Not. Roy. Astron. Soc. **341**, 1311 (2003), arXiv:astro-ph/0207664 [astro-ph].
- [35] C. Orban and D. H. Weinberg, Phys. Rev. D **84**, 063501 (2011), arXiv:1101.1523 [astro-ph.CO].
- [36] T. Baertschiger, M. Joyce, A. Gabrielli, and F. Sylos Labini, Phys. Rev. E **75**, 021113 (2007), arXiv:cond-mat/0607396 [cond-mat.stat-mech].
- [37] T. Baertschiger, M. Joyce, A. Gabrielli, and F. Sylos Labini, Phys. Rev. E **76**, 011116 (2007), arXiv:cond-mat/0612594 [cond-mat.stat-mech].
- [38] T. Baertschiger, M. Joyce, F. Sylos Labini, and B. Marcos, Phys. Rev. E **77**, 051114 (2008), arXiv:0711.2219 [cond-mat.stat-mech].
- [39] N. Makino, M. Sasaki, and Y. Suto, Phys. Rev. D **46**, 585 (1992).
- [40] R. Scoccimarro and J. A. Frieman, Astrophys. J. **473**, 620 (1996), arXiv:astro-ph/9602070 [astro-ph].
- [41] M. Peloso and M. Pietroni, JCAP **2013** (5), 031, arXiv:1302.0223 [astro-ph.CO].
- [42] R. Takahashi, Prog. Theor. Phys. **120**, 549 (2008), arXiv:0806.1437 [astro-ph].
- [43] M. Garny and P. Taule, JCAP **2022** (9), 054, arXiv:2205.11533 [astro-ph.CO].
- [44] M. Fasiello, T. Fujita, and Z. Vlah, Phys. Rev. D **106**, 123504 (2022), arXiv:2205.10026 [astro-ph.CO].
- [45] Springel and Volker, Mon. Not. Roy. Astron. Soc. **364** 1105-1134 10.1111/j.1365-2966.2005.09655.x (2005), astro-ph/0505010v1.
- [46] D. Benhaiem, M. Joyce, and F. Sicard, Mon. Not. R. Astron. Soc. **429**, 3423 (2013), arXiv:1211.6642 [astro-ph.CO].
- [47] D. Benhaiem, *Non linear gravitational clustering in scale free cosmological models*, Ph.D. thesis, Université Pierre et Marie Curie (2013).
- [48] E. Bertschinger, arXiv e-prints , astro-ph/9506070 (1995), arXiv:astro-ph/9506070 [astro-ph].
- [49] M. Joyce and B. Marcos, Phys. Rev. D **75**, 063516 (2007), arXiv:astro-ph/0410451 [astro-ph].
- [50] S. R. Knollmann, C. Power, and A. Knebe, Mon. Not. R. Astron. Soc. **385**, 545 (2008), arXiv:0801.1851 [astro-ph].
- [51] S. Colombi, A. Jaffe, D. Novikov, and C. Pichon, Mon. Not. R. Astron. Soc. **393**, 511 (2009), arXiv:0811.0313 [astro-ph].
- [52] M. Bottaccio, L. Pietronero, A. Amici, P. Miocchi, R. Capuzzo Dolcetta, and M. Montuori, Phys. A: Stat. Mech. Appl. **305**, 247 (2002), arXiv:cond-mat/0111472 [cond-mat.stat-mech].
- [53] W. R. Inc., Mathematica, Version 13.2, champaign, IL, 2022.